Since January 2020 Elsevier has created a COVID-19 resource centre with free information in English and Mandarin on the novel coronavirus COVID-19. The COVID-19 resource centre is hosted on Elsevier Connect, the company's public news and information website.

Biosensors and Bioelectronics 170 (2020) 112656

Contents lists available at ScienceDirect

Biosensors and Bioelectronics

journal homepage: http://www.elsevier.com/locate/bios

An integrated system of air sampling and simultaneous enrichment for rapid biosensing of airborne coronavirus and influenza virus

Hyeong Rae Kim, Sanggwon An, Jungho Hwang *

School of Mechanical Engineering, Yonsei University, Seoul 03722, Republic of Korea

ARTICLE INFO

Keywords:
Coronavirus
Airborne virus
Airborne virus monitoring
Aerosol-to-hydrosol sampling
Electrostatic air sampler
Virus enrichment

ABSTRACT

Point-of-care risk assessment (PCRA) for airborne viruses requires a system that can enrich low-concentration airborne viruses dispersed in field environments into a small volume of liquid. In this study, airborne virus particles were collected to a degree above the limit of detection (LOD) for a real-time quantitative reverse transcription polymerase chain reaction (qRT-PCR). This study employed an electrostatic air sampler to capture aerosolized test viruses (human coronavirus 229E (HCoV-229E), influenza A virus subtype H1N1 (A/H1N1), and influenza A virus subtype H3N2 (A/H3N2)) in a continuously flowing liquid (aerosol-to-hydrosol (ATH) enrichment) and a concanavalin A (ConA)-coated magnetic particles (CMPs)-installed fluidic channel for simultaneous hydrosol-to-hydrosol (HTH) enrichment. The air sampler's ATH enrichment capacity (EC) was evaluated using the aerosol counting method. In contrast, the HTH EC for the ATH-collected sample was evaluated using transmission-electron-microscopy (TEM)-based image analysis and real-time qRT-PCR assay. For example, the ATH EC for HCoV-229E was up to 67,000, resulting in a viral concentration of 0.08 PFU/mL (in a liquid sample) for a viral epidemic scenario of 1.2 PFU/m^3 (in air). The real-time qRT-PCR assay result for this liquid sample was "non-detectable" however, subsequent HTH enrichment for 10 min caused the "non-detectable" sample to become "detectable" (cycle threshold (CT) value of 33.8 ± 0.06).

1. Introduction

Zoonosis has historically inflicted significant loss of life and high social costs on humankind by way of human exposure to both wild animals and livestock. Ironically, it has also accelerated the development of biomedicines, such as vaccines and antibody drugs. However, severe acute respiratory syndrome coronavirus (SARS-CoV), the Middle-East respiratory syndrome coronavirus (MERS-CoV), the novel coronavirus in 2019 (SARS-CoV2), and influenza A virus (H1N1) are powerful and infectious viruses that have emerged in the 21st century. SARS-CoV affected >8000 persons worldwide and was responsible for >700 deaths during an outbreak in 2002 (Peiris et al., 2004). MERS-CoV affected >2200 persons in 27 countries with an associated mortality rate of 35% (Nassar et al., 2018). The number of persons worldwide infected with SARS-CoV2 is approximately 30 million thus far (as of Sep. 16, 2020). The US Centers for Disease Control and Prevention (CDC) estimates that the influenza virus has caused 9.2–35.6 million illnesses, 140,000–710,000 hospitalizations, and 12,000–56,000 deaths annually since 2010 (CDC, 2020). Efforts to prevent the spread of epidemics have been ongoing for centuries. However, effective methods apart from isolating the infected, sterilizing suspected contaminations, wearing a mask, and washing hands have not yet been created.

The monitoring of airborne biological particles (bioaerosols such as bacteria, fungi, and viruses) has continued for decades in an effort to prevent the spread of infectious diseases caused by droplets or airborne viruses. However, few techniques exist for the monitoring of airborne viruses. The most commonly used viral monitoring method is quantitative reverse transcription polymerase chain reaction (qRT-PCR), which is based on the detection of the target gene with high reliability. The limit of detection (LOD) for a real-time qRT-PCR device in the market is usually thousands of viral genome copies per 1 mL of liquid (Drosten et al., 2002; Corman et al., 2020). The first step for monitoring an airborne virus is to capture it in a liquid because a liquid-based detection scheme can be applied in real-time qRT-PCR and other bioanalytical techniques (e.g., nucleic acid detection, immunoassay, and identification with cell culturing). However, a relatively low concentration of the virus exists in air (10^3–10^4 of viral genome copies per 1 m^3 of air) even during an influenza epidemic and COVID-19 pandemic in

* Corresponding author. School of Mechanical Engineering Yonsei University, 134 Shinchon-dong, Seodaemun-gu, Seoul, Republic of Korea.
E-mail addresses: khr1410@yonsei.ac.kr (H.R. Kim), dkstkdrnjs@naver.com (S. An), hwangjh@yonsei.ac.kr (J. Hwang).

https://doi.org/10.1016/j.bios.2020.112656
Received 17 July 2020; Received in revised form 16 September 2020; Accepted 24 September 2020
Available online 26 September 2020

indoor environments, which complicates the monitoring of airborne virus (Yang et al., 2011; Lindsley et al., 2010; Chia et al., 2020; Santarpia et al., 2020). A long air-sampling time and complex pretreatments are required to prepare virus samples above the LOD of a real-time qRT-PCR.

Developing a point-of-care risk assessment (PCRA) system to enrich the low-concentration airborne viruses scattered in field environments into a small volume of liquid to a concentration above the LOD of real-time qRT-PCR is vital for preventing fatalities from airborne viruses and stopping their spread. Accordingly, an aerosol-to-hydrosol (ATH) enrichment capacity (EC) of 10^5–10^6-fold (from 10^3–10^4 of viral genome copies per 1 m^3 of air in a viral epidemic scenario to 10^3 of viral genome copies per 1 mL of liquid) is required. For high EC, a high viral collection efficiency with a high air-sampling flow rate and small volume of the liquid sample are essential.

However, it is practically difficult for an air sampler to meet all these requirements for a high EC. For example, the Airborne Sample Analysis Platform (ASAP) 2800 (Thermo Scientific, USA) bioaerosol sampler is a commercial device that cannot collect airborne particles smaller than 1 μm, which accounts for 20–60% of the indoor airborne particles that contain viruses (Thermo scientific; Yang et al., 2011). Lee et al. (2016) reported a disposable bio-precipitator for capturing and enriching airborne bacteria into small volume of liquid (15 μL). The National Institute for Occupational Safety and Health (NIOSH) bioaerosols sampler was developed to sample virus-containing particles smaller than 1 μm. However, an additional recovery step is required for bioassaying because the NIOSH bioaerosols sampler collects airborne particles smaller than 1 μm on a filter (Cao et al., 2011). The SKC BioSampler is a commercial air-sampling device that captures bioaerosols in 20 mL of liquid such that the liquid sample can be easily used in a bioanalytical assay. However, its EC is only 62.5, which is inappropriate for use in field environments. The low collection efficiency for virus-sized particles (100 nm) and the relatively large volume of collection liquid (20 mL) for the SKC BioSampler results in a low EC (Hogan et al., 2005).

Lab-designed air samplers have been developed for a higher enrichment capacity (EC). Wubulihairen et al. (2015) introduced an ATH sampler that could apply an inertia impaction method where the EC was 835 for 100-nm particles. Hong et al. (2016) studied an electrostatic particle concentrator (EPC) that could capture airborne viruses in a liquid volume of 0.5 mL; however, the EPC had a low EC of 8750 for a 100-nm airborne virus.

We have developed a field-applicable system to address these challenges (high viral collection efficiency with a high air-sampling flow rate and a small volume of liquid sample for high EC) that collects airborne viruses in a liquid and simultaneously enriches the collected viruses above the LOD of a real-time qRT-PCR device. We have previously reported a method for ATH sampling and the simultaneous HTH enrichment of airborne bacteria (Kim et al., 2020). An electrostatic air sampler and an enrichment channel immobilized with concanavalin A (ConA)--coated magnetic particles (CMPs) were applied to achieve a high EC. With this method, the low-concentration aerosolized *Staphylococcus aureus* (4.75×10^6 CFU per 1 m^3 of air, CFU: colony-forming unit) bacteria were converted into highly enriched bacteria (5.66×10^6 CFU per 1 mL of liquid).

In this paper, our method is expanded for airborne viruses with a system that integrates an ATH sampler and a HTH enrichment channel. Even though a liquid sample obtained via the ATH collection of virus particles of very low concentration in air is "non-detectable" in real-time qRT-PCR analysis, we demonstrate that subsequent HTH enrichment can cause a "non-detectable" sample to become "detectable." Human coronavirus 229E (HCoV-229E), Influenza A virus subtype H1N1 (A/H1N1), and Influenza A virus subtype H3N2 (A/H3N2) were used as test viruses. The ATH enrichment capacities of the viruses were evaluated using an aerosol counting method. Transmission electron microscopy (TEM) and real-time qRT-PCR were applied for the reliable verification of HTH EC.

2. Materials and methods

2.1. Aerosol-to-hydrosol (ATH) collection of atomized viruses

The aerosol collection efficiency of our ATH sampler was tested at various air flow rates (4, 6, 8, and 10 L/min) and applied voltages (−7, −6, −5, +5, +6, and +7 kV). Three infectious airborne viruses (HCoV-229E, A/H1N1, and A/H3N2) were used to evaluate our method. Fig. 1a is an experimental schematic for the sampling of airborne viruses and the performance evaluation of simultaneous enrichment. Each virus stock was mixed with 45 mL of deionized water after thawing on an ice pack. A wide range of concentrations were prepared for each virus species to evaluate our system's performance.

The mixed solution (total volume: 50 mL) was atomized using a Collison-type atomizer (9302, TSI Inc., USA). The flow rate of clean air supplied to the atomizer was 2 L/min. A diffusion dryer was used to remove the dampness from the atomized viruses. A Boltzmann charge distribution was induced after the demoisturized viruses were passed through a neutralizer (Soft X-ray charger 4530, HCT, Republic of Korea). The neutralized viruses were diluted with clean air and placed into the ATH sampler, whose flow rate was regulated by an air pump. The total air-sampling flow rate of the ATH sampler was 4–10 L/min.

The virus aerosols entering the ATH sampler were charged via air ions created from the tips of two discharge electrodes by corona discharge and collected on a ground electrode covered by continuously provided phosphate-buffered saline (PBS, PR2004–100–72, Biosesang, Republic of Korea). PBS was used to minimize any damage that might be caused by corona discharge during the ATH sampling of viruses (Piri et al., 2020). The collection efficiency of the ATH sampler ($\eta_{collection}$) for airborne virus was calculated as follows:

$$\eta_{collection} = 1 - \frac{C_{on}}{C_{off}} \quad (1)$$

where C_{on} and C_{off} are the numerical concentrations of the airborne viruses counted at the downstream of the ATH sampler with a scanning mobility particle sizer (SMPS, TSI, USA) when the voltage applied to the sampler was on and off, respectively. SMPS consists of a classifier (3080, TSI Inc., USA), a differential mobility analyzer (DMA, 3081, TSI Inc., USA), an aerosol charge neutralizer (Soft X-ray charger 4530, HCT, Republic of Korea), and a condensation particle counter (CPC, 3775, TSI Inc., USA). The various-size aerosol particles entering the DMA were sorted by particle size using the classifier controller. The aerosol particles entering the CPC were condensed with butanol to spur growth, the particles were passed through a laser, and the number of particles was counted.

When the viruses initially dispersed in air were captured on a liquid, the viral concentration would naturally increase because the volume decreased from air to liquid. The enrichment capacity by the ATH collection process is defined as follows:

$$EC_{ATH} = \frac{Q_A \times \eta_{collection}}{Q_L} \quad (2)$$

where Q_A is the air-sampling flow rate of the ATH sampler and Q_L is the flow rate of the carrier liquid (100 μL/min in this study) supplied to the enrichment channel. After the ATH collection of virus particles, each collected viral sample was assayed with real-time qRT-PCR to quantify the viral concentration.

2.2. Hydrosol-to-hydrosol (HTH) enrichment of collected viruses

The ATH-collected viruses were directly delivered to the enrichment channel for HTH enrichment. The viruses that entered the channel were adsorbed to previously immobilized CMPs. The process of immobilizing CMPs is described in detail in Supplementary Data. The HTH enrichment test was conducted for 1–10 min. After the test, magnetic blocks

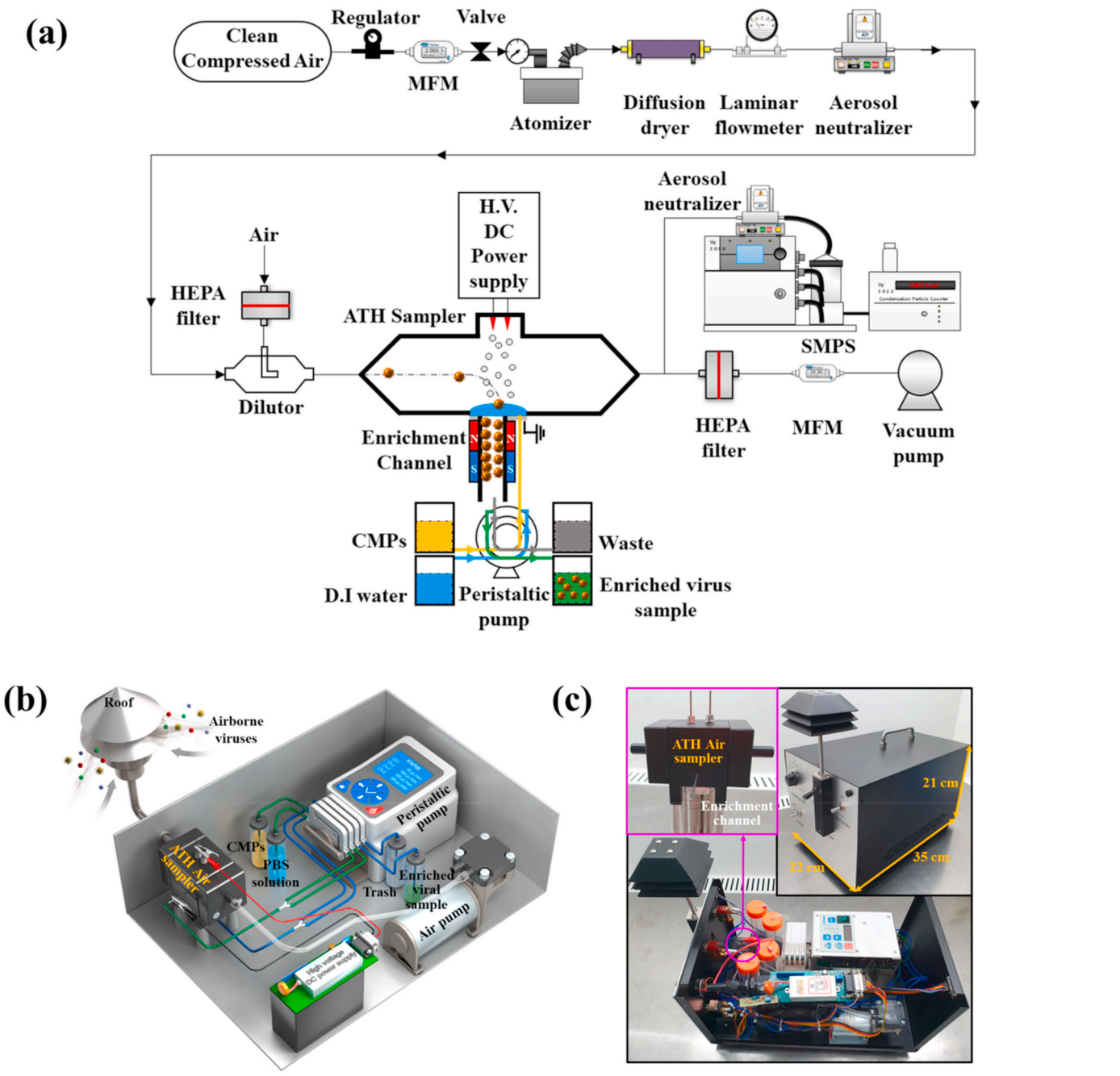

Fig. 1. (a) Overall experimental setup for airborne virus sampling and enrichment tests. (b) 3D schematic and (c) photograph of an integrated system for sampling and simultaneous enrichment for rapid PCRA.

surrounding the channel were eliminated and fresh PBS solution was injected into the channel to flush out the enriched viruses for analysis. Fluorescein isothiocyanate (FITC)-conjugated ConA (C7642, Sigma-Aldrich, USA) was used to observe the process of coating and flushing out the CMPs with a confocal microscope (LSM980, Carl Zeiss, Germany). Fig. S1 of the Supplementary Data depicts the fluorescence microscopic images of liquid samples obtained with and without installing the CMPs on the inside wall of the enrichment channel. Fluorescent spots that represent FITC-conjugated ConA were confirmed for the sample obtained with the CMPs installed. No fluorescent spots were observed for the sample obtained without CMPs. Therefore, we confirmed that the CMPs were maintained in the enrichment channel during the HTH enrichment of ATH-collected viruses.

The HTH enrichment performance was visually confirmed via TEM (JEM-1011, JEOL, Japan) using the negative staining technique. Each liquid sample was washed using a PBS buffer and 4 μL of the washed sample was placed on a TEM grid (3420C-CF, SPI Supplies, USA). After 30 s, the excess of the sample was wicked away using filter paper (01531055, ADVANTEC, USA). Four microliters of 1% uranyl acetate (E22400–1, Science Services, Germany) was placed on the grid for 15 s and filter paper was used to remove the reagent and then 4 μL of ultrapure water was applied to wash the residue. The negative stained virus was observed after drying for 30 min at 20 °C.

The HTH enrichment performance was also confirmed by real-time qRT-PCR using a PikoReal Real-Time PCR System (TCR0096, Thermo Scientific, USA). The RNA of each virus sample was extracted using a Power Prep Quick RNA extraction kit (E0014, Kogenebiotech, Republic of Korea) and the extracted RNA samples were mixed using real-time RT-

PCR kits. PowerChek Pandemic H1N1/H3N2 Real-time PCR Kit Ver. 1.0 (R3410, Kogenebiotech, Republic of Korea) was used to assay A/H1N1 and A/H3N2. A Coronavirus 229E/OC43/NL63/HKU1 Real-Time PCR Kit (64000F, Kogenebiotech, Republic of Korea) was used to assay HCoV-229E. All RNA extraction and real-time qRT-PCR assays were carried out following the manufacturer's instructions. The cycling protocol for real-time qRT-PCR was as follows: a Uracil DNA Glycosylase activation step at 50 °C for 30 min, an initial denaturation step at 95 °C for 10 min, 40 or 45 cycles of denaturation at 95 °C for 15 s, and annealing and extension at 60 °C for 1 min. All real-time qRT-PCR assays were repeated three times.

Based on the cycle threshold (CT) value from real-time qRT-PCR assay, the initial concentration of the target RNA can be calculated. To quantify the HTH EC (EC_{HTH}), the following equation was reported by Kim et al. (2020):

$$EC_{HTH} = (1+E)^{(CT_{Before} - CT_{After})} \quad (3)$$

where CT_{Before} and CT_{After} are the CT values before and after the HTH enrichment. E is the PCR reaction efficiency (E = 1 for 100%). The total enrichment capacity (EC_T), considering both the ATH and HTH enrichments, is defined as follows:

$$EC_T = EC_{ATH} \times EC_{HTH} \quad (4)$$

2.3. An integrated system of sampling and simultaneous enrichment of airborne viruses

Fig. 1b and c illustrate a 3D schematic and a picture of our integrated system, respectively. The system consists of a roof, which is an inlet to the system, an ATH electrostatic air sampler, a power supply module, a peristaltic pump, a vacuum pump, and four containers. The size and weight of the system are 22 × 35 × 21 cm (width × length × height) and 5 kg, respectively.

3. Results and discussion

3.1. Aerosol-to-hydrosol (ATH) collection of atomized viruses

Fig. 2a illustrates the size distributions of the atomized HCoV-229E, A/H1N1, and A/H3N2 as measured by SMPS. The peak mobility diameter of the influenza viruses (A/H1N1 and A/H3N2) was approximately 95 nm, which was similar to that of previously reported studies that observed the influenza virus using an electron microscope (Nayak et al., 2009; Kang et al., 2015). Fig. 2a depicts that the diameter of HCoV-229E

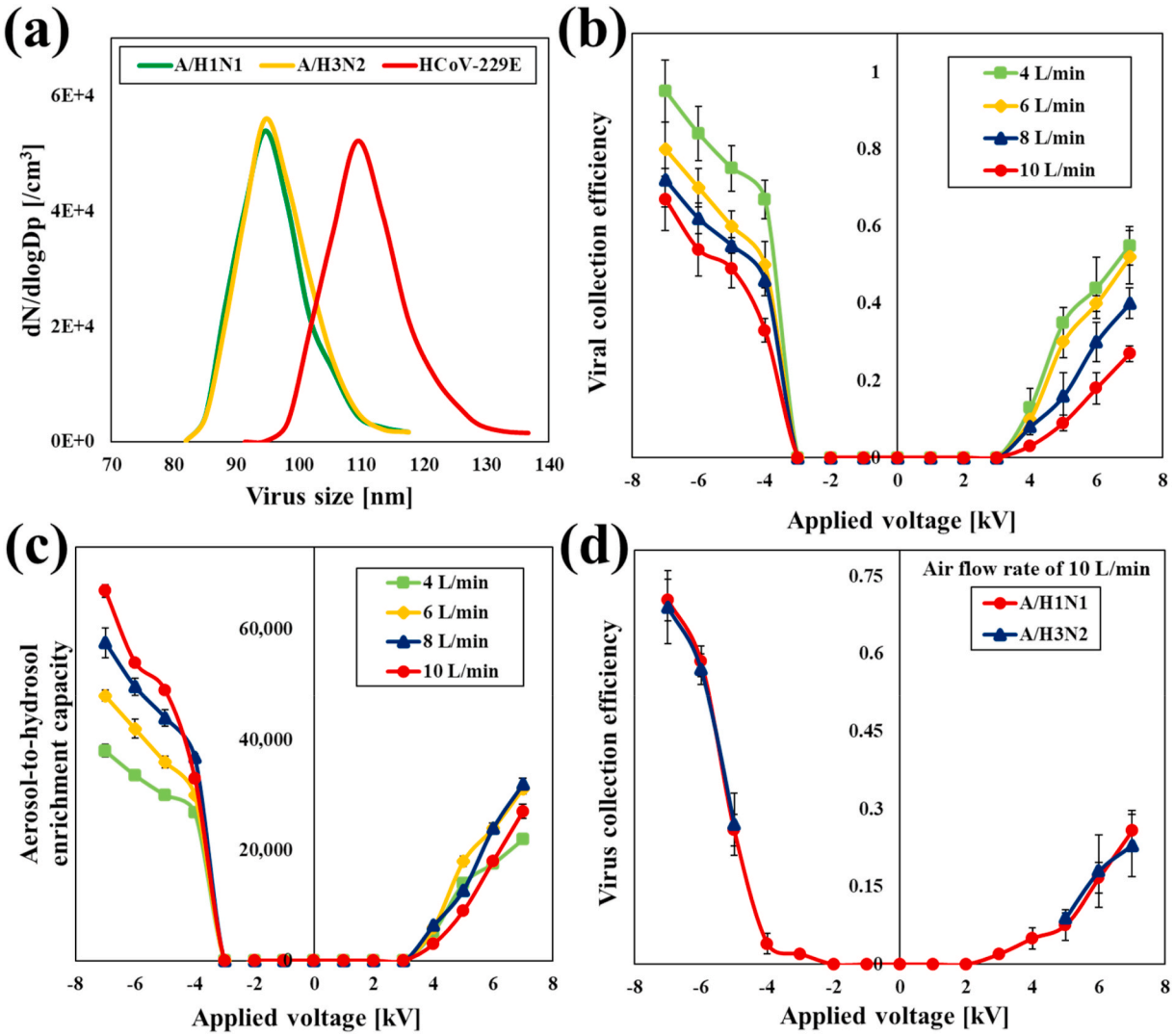

Fig. 2. (a) Size distributions of airborne viruses (HCoV-229E, A/H1N1, and A/H3N2) as measured by SMPS, (b) Virus (HCoV-229E) collection efficiency according to varying air flow rates and applied voltages, (c) ATH EC according to varying air flow rates and applied voltages for HCoV-229E, (d) virus (A/H1N1, and A/H3N2) collection efficiency according to varying applied voltages (10 L/min of air flow rate).

had a size range of 90–140 nm (109 nm at the peak). The diameter of the novel coronavirus SARS-CoV-2 varied from 60 to 140 nm (Liu et al., 2020; Zhu et al., 2020).

Fig. 2b illustrates the collection efficiencies of the ATH sampler for HCoV-229E with various air-sampling flow rates and applied voltages. The wall loss of virus particles by diffusion in the tube and ATH sampler was smaller than 1%. Details are described in the Supplementary Data. Fig. 2b reveals that the collection efficiency increased with an applied voltage but decreased with the air-sampling flow rate at all applied voltages higher than the corona starting voltages (±3 kV). According to the classical aerosol charging theory (Hinds, 1999), the particle collection efficiency increases with the particle charge, which increases with the increase of the gaseous ion concentration (See Eq. (d)–(h) in the Supplementary Data). Fig. S2 of the Supplementary Data shows that a negative discharge generates a higher current than a positive discharge for the same magnitude of an applied voltage. The ion concentration increases with the electrical current (See Eq. (i) in the Supplementary Data). Therefore, the collection efficiency is higher under an applied negative voltage than under an applied positive voltage of the same magnitude. Additionally, the number of particle charges is proportional to the residence time of the particle exposed to the electric field (See Eq. (f)-(h) in the Supplementary Data). As the air flow rate increases, the time during which particles are exposed to the electric field becomes shorter; therefore, they are not sufficiently charged, which results in a decrease in the aerosol collection efficiency. When the air flow rates entering the ATH sampler increased from 6 to 8 and 10 L/min, the residence times of virus particle decreased from 0.024 to 0.018 and 0.014 s, respectively. Additionally, even if the temperature of the ambient air changed from 0 °C to 40 °C for example, the viral collection efficiency of the ATH sampler increased as much as 0.4% according to aerosol theory (Hinds, 1999). Details are described in Supplementary Data. Nouri et al. (2012) showed that the electrical current rarely changes for a negative corona discharge when the relative humidity increases from 10% to 99%.

Fig. 2c illustrates the EC_{ATH} of our ATH sampler for HCoV-229E with various applied voltages and air-sampling flow rates. The EC_{ATH} was the highest when the applied voltage was −7 kV and the air-sampling flow rate was 10 L/min. Therefore, we selected an applied voltage and air-sampling flow rate of −7 kV and 10 L/min, respectively, as the airborne virus sampling conditions.

Fig. 2d shows that the collection efficiency of the ATH sampler for airborne viruses was independent of the subtype species of the viruses. The collection efficiency increased with the electrical migration velocity, which depends on particle size (Hinds, 1999). Because the A/H1N1 and A/H3N2 viruses are similar in size, the collection efficiencies for these viruses were similar (Fig. 2a). The virus collection efficiency of the ATH sampler as measured with the aerosol counting method was compared to that measured with plaque assay. For this comparison, MS2 bacteriophages were used since the morphology of MS2 bacteriophages is similar to that of pathogenic viruses, including the foot-and-mouth disease (FMD) virus, rhinovirus, and poliovirus (Hong et al., 2016). The details are presented in the Supplementary Data.

For these conditions, the ATH enrichment capacities (EC_{ATH}) for HCoV-229E, A/H1N1, and A/H3N2 were calculated to be 67,000, 70,400, and 69,000, respectively (Eq. (2)). Plaque assays were performed for the ATH-collected virus samples. Plaque assay results are depicted in Table S1 of Supplementary Data in units of PFU/mL (PFU: plaque-forming unit). Real-time qRT-PCR analyses were conducted for the ATH-collected samples. Table S1 also presents the corresponding cycle threshold (CT) values assayed with the PCR. For HCoV-229E, for example, three different liquid (hydrosol) samples (1.3×10^4, 9.8×10^2, and 0.6×10^1 PFU/mL) that were obtained by ATH collection were "detectable." However, when the concentration of a sample was as low as 0.08 PFU/mL, the PCR analysis results were "non-detectable."

Table S1 presents a wide range of concentrations of virus aerosols (PFU/m^3) for each species. Aerosol concentrations of 1.2, 5.6×10^1 and 5.5×10^1 PFU/m^3 (marked with * in Table S1) for HCoV-229E, A/H1N1, and A/H3N2, respectively, were selected from a previous study by Yang et al. (2011). Then, the corresponding concentrations of 0.08, 3.94, and 3.8 PFU/mL, respectively, for HCoV-229E, A/H1N1, and A/H3N2, were calculated by multiplying the aerosol concentration (PFU/m^3) by the EC_{ATH} for each virus species. Other hydrosol concentrations were determined using the same approach for the assumed aerosol concentrations, respectively.

Yang et al. (2011) reported that the concentration of airborne influenza virus in viral epidemic scenarios range from 13 to 82 $TCID_{50}/m^3$ (equivalent to 5.8×10^3 to 3.7×10^4 RNA genome copies/m^3). We selected 80 $TCID_{50}/m^3$ (equivalent to 3.6×10^4 RNA genome copies/m^3) to be the viral aerosol concentration for simulating the viral epidemic scenario. 3.6×10^4 RNA genome copies/m^3 is equivalent to 1.2 PFU/m^3 for HCoV-229E (1 PFU/mL = 3×10^4 RNA/mL) (Corman et al., 2012). 80 $TCID_{50}/m^3$ can be converted to 56 PFU/m^3 and 55 PFU/m^3 for A/H1N1 and A/H3N2, respectively (1 $TCID_{50}$/mL = 0.7 PFU/mL for A/H1N1 and 1 $TCID_{50}$/mL = 0.69 PFU/mL for A/H3N2) (Yang et al., 2011; van Baalen et al., 2017).

3.2. Hydrosol-to-hydrosol (HTH) enrichment of collected viruses

Fig. 3a illustrates the real-time qRT-PCR amplification curves with various HTH enrichment times (0, 1, 5, and 10 min) for 6 PFU/mL of the HCoV-229E sample. The CT values were advanced from the CT value of the ATH sample (32.6) with the HTH enrichment time. Consequently, 1, 5, and 10 min of HTH enrichment advanced the CT values to 2.1 ± 0.14 (from 32.6 to 30.5 ± 0.14), 3.4 ± 0.09 (from 32.6 to 29.2 ± 0.09), and 5.5 ± 0.04 (from 32.6 to 27.1 ± 0.04), respectively (Fig. 3b). Therefore, the HTH enrichment capacities for 1, 5, and 10 min of enrichment were 4.29, 10.56, and 45.25, respectively (obtained with Eq. (3)). Fig. 3c illustrates that the total enrichment capacities (EC_T) were 287,235, 707,256, and 3,032,074, respectively, for HTH enrichment times of 1, 5, and 10 min (obtained with Eq. (4)). The ATH EC (EC_{ATH}) of the ATH sampler for HCoV-229E was 67,000.

Fig. 3d, e, and f depict the real-time qRT-PCR amplification curves before and after 10 min of HTH enrichment for various concentrations of HCoV-229E, A/H1N1, and A/H3N2 samples, respectively. For the blue dotted curve in Fig. 3d, for example, the liquid sample of 1.3×10^4 PFU/mL obtained by ATH collection (CT_{Before} = 21.2 ± 0.12) became a full blue curve (CT_{After} = 19.1 ± 0.14) after 10 min of HTH enrichment. Notably, the liquid sample of 0.08 PFU/mL (red dotted curve), which was "non-detectable" with PCR analysis, became a "detectable" sample (full red curve) after the HTH enrichment process. Table S2 of the Supplementary Data presents the CT values of the HTH-enriched samples with various concentrations of HCoV-229E, A/H1N1, and A/H3N2 samples. A higher HTH EC was obtained for a lower aerosol concentration for all tested virus samples. This trend was previously reported by Jing et al. (2019) who found that a bacterial sample of 10^3 cells/mL was 12-fold higher in its enrichment effect than a bacterial sample 10^5 cells/mL in a microfluidic chip. Our previous study also found that the HTH enrichment effect for an *S. aureus* sample of 3.8×10^5 CFU/mL was eight-fold higher than for an *S. aureus* sample of 1.8×10^7 CFU/mL (Kim et al., 2020). We carried out experiments to investigate whether the presence of dust particles and other virus species (A/H1N1) can affect the hydrosol-to-hydrosol enrichment for HCoV-229E. Details are described in Supplementary Data.

Fig. 3g illustrates the total enrichment capacities (EC_T) for samples of three different concentrations of aerosolized HCoV-229E, A/H1N1, and A/H3N2 (obtained with Eq. (4)) after 10 min of HTH enrichment. The total enrichment capacity (EC_T) for each sample was calculated with Eq. (4) by multiplying the EC_{ATH} (see Table S1) by the EC_{HTH} (see Table S2). The total enrichment capacities were 3,032,074, 2,414,491, and 2,536,326, respectively, for the HCoV-229E, A/H1N1, and A/H3N2 samples with concentrations of 9.0×10^1 PFU/m^3 (0.6×10^1 PFU/mL),

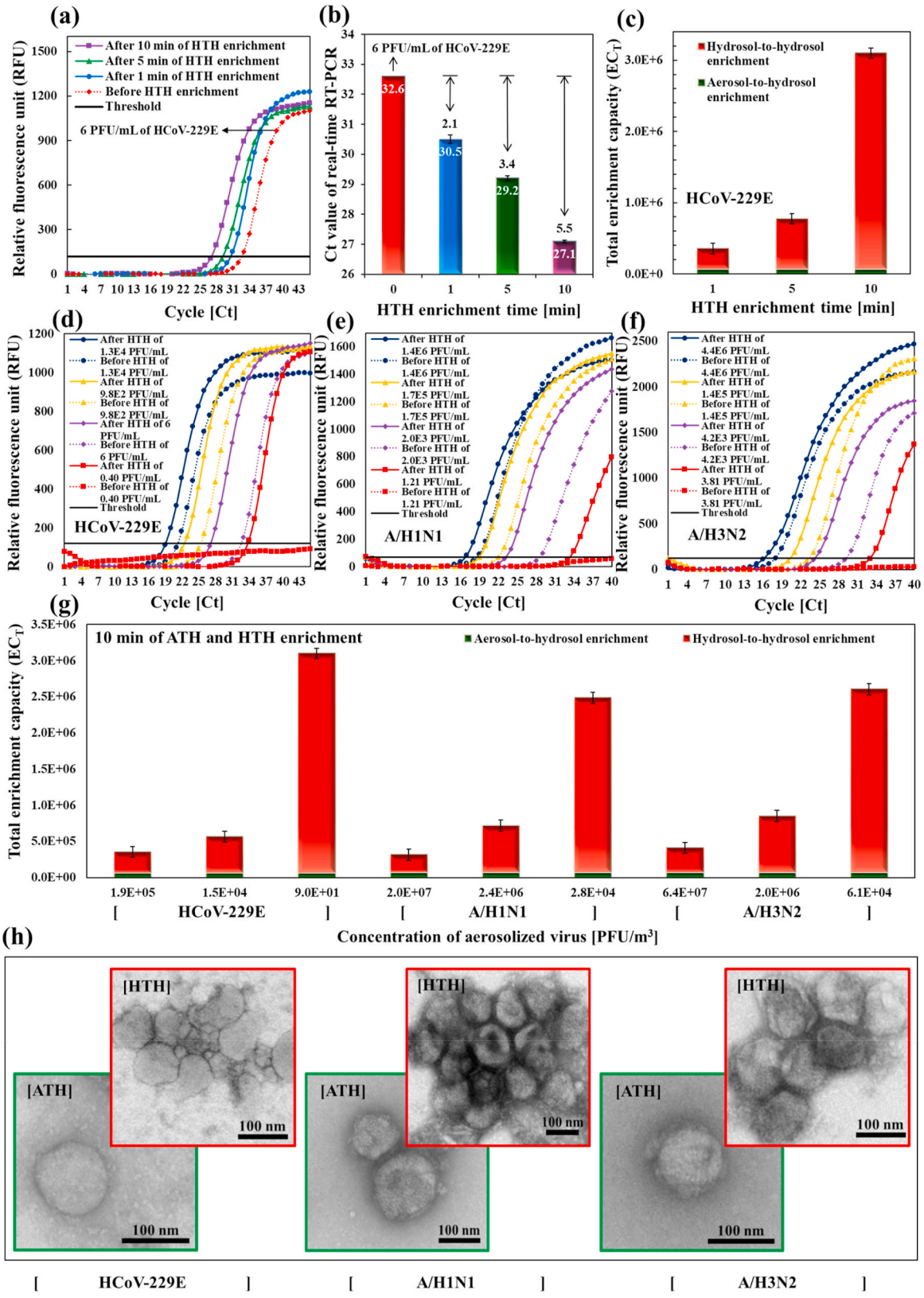

Fig. 3. (a) Real-time qRT-PCR amplification curves with various HTH enrichment times (0, 1, 5, 10 min) for 6 PFU/mL of HCoV-229E. (b) Corresponding CT values. (c) Total enrichment capacities for HCoV-229E with various HTH enrichment times. Real-time qRT-PCR amplification curves; before and after HTH enrichment for various concentrations of (d) HCoV-229E, (e) A/H1N1, and (f) A/H3N2 samples. The dotted curves, representing ATH-collected viruses, became full curves after HTH enrichment (e.g., red dotted curves became full red curves after HTH enrichment). (g) Total enrichment capacities for HCoV-229E, A/H1N1, and A/H3N2 with different concentrations of aerosolized viruses. (h) TEM images of HCoV-229E, A/H1N1, and A/H3N2 samples with an ATH sampling method (green box) and an HTH enrichment method after ATH sampling (red box).

2.8×10^4 PFU/m^3 (2.0×10^3 PFU/mL), and 6.1×10^4 PFU/m^3 (4.2×10^3 PFU/mL). These EC_T values were higher than 10^6, which is reported as the enrichment capacity (from 10^5 to 10^6-folds) required for real-time qRT-PCR detection in a viral epidemic field environment (Yang et al., 2011).

Fig. 3h depict TEM images of HCoV-229E, A/H1N1, and A/H3N2 with an ATH collection method (green box) and with an HTH enrichment method (red box) after ATH collection. After HTH enrichment using the CMPs, the viruses were more concentrated and agglomerated than those without HTH enrichment.

4. Conclusions

In this study, an air sampler and an additional enrichment channel-integrated hand-held system was developed for Point-of-care viral risk assessment in field environments. The aerosol counting method and real-time qRT-PCR assay showed that our system can enrich the aerosolized HCoV-229E, A/H1N1, and A/H3N2 particles more than 10^6-fold. The most impressive feature of our study is that the non-detectable ATH collected viral samples in a viral epidemic scenario turned into detectable samples in 10 min with an HTH enrichment process. Therefore, our system can be used in field environments where the concentration of airborne viruses is very low for the efficient and rapid monitoring of airborne viruses. The limitation of our system is that preparation steps for additional materials (CMPs) are needed for HTH enrichment. Therefore, in the future, we aim to develop an air sampler with an ATH enrichment capacity that is high enough without the effects of an enrichment channel.

The air sampling time taken for monitoring of airborne coronavirus and influenza virus in viral epidemic scenario can be significantly reduced (<10 min) owing to the enrichment capacity (>10^6).

CRediT authorship contribution statement

Hyeong Rae Kim: Conceptualization, Investigation, Writing - original draft. **Sanggwon An:** Investigation, Validation. **Jungho Hwang:** Funding acquisition, Writing - review & editing, Supervision.

Declaration of competing interest

The authors declare that they have no known competing financial interests or personal relationships that could have appeared to influence the work reported in this paper.

Acknowledgments

This research was supported by BioNano Health-Guard Research Center funded by the Ministry of Science and ICT (MSIT) of Korea as Global Frontier Project (Grant number H-GUARD_2013M3A6B2078959).

Appendix A. Supplementary data

Supplementary data to this article can be found online at https://doi.org/10.1016/j.bios.2020.112656.

References

Cao, G., Noti, J.D., Blachere, F.M., Lindsley, W.G., Beezhold, D.H., 2011. J. Environ. Monit. 13 (12), 3321–3328.
CDC. https://www.cdc.gov/flu/about/disease/burden.htm. (Accessed 12 September 2020).
Chia, P.Y., Coleman, K.K., Tan, Y.K., Ong, S.W.X., Gum, M., Lau, S.K., Sutjipto, S., Lee, P. H., Son, T.T., Young, B.E., Milton, D.K., Gray, G.C., Schuster, S., Barkham, T., De, P. P., Vasoo, S., Chan, M., Ang, B.S.P., Tan, B.H., Leo, Y.-S., Ng, O.-T., Wong, M.S.Y., Marimuthu, K., 2020. medRxiv.
Corman, V.M., Landt, O., Kaiser, M., Molenkamp, R., Meijer, A., Chu, D.K., Bleicker, T., Brünink, S., Schneider, J., Schmidt, M.L., Mulders, D.G., Haagmans, B.L., Veer, B.V. D., Brink, S.V.D., Wijsman, L., Goderski, G., Romette, J., Ellis, J., Zambon, M., Peiris, M., Gooddens, H., Reusken, C., Koopmans, M.P., Drosten, C., 2020. Euro Surveill. 25 (3), 2000045.
Drosten, C., Göttig, S., Schilling, S., Asper, M., Panning, M., Schmitz, H., Günther, S., 2002. J. Clin. Microbiol. 40 (7), 2323–2330.
Hinds, W.C., 1999. Aerosol Technology: Properties, Behavior, and Measurement of Airborne Particles. John Wiley & Sons, New Jersey.
Hogan Jr., C.J., Kettleson, E.M., Lee, M.H., Ramaswami, B., Angenent, L.T., Biswas, P., 2005. J. Appl. Microbiol. 99 (6), 1422–1434.
Hong, S., Bhardwaj, J., Han, C., Jang, J., 2016. Environ. Sci. Technol. 50 (22), 12365–12372.
Jing, W., Zhao, W., Liu, S., Li, L., Tsai, C.T., Fan, X., Wu, W., Li, J., Yang, X., Sui, G., 2013. Anal. Chem. 85 (10), 5255–5262.
Kang, P., Schein, P., Serey, X., O'Dell, D., Erickson, D., 2015. Sci. Rep. 5, 12087.
Kim, H.R., An, S., Hwang, J., 2020. ACS Sensors 5 (9), 2763–2771.
Lee, E.H., Chua, B., Son, A., 2016. Biosens. Bioelectron. 83, 205–212.
Lindsley, W.G., Blachere, F.M., Davis, K.A., Pearce, T.A., Fisher, M.A., Khakoo, R., Davis, S.M., Rogers, M.E., Thewlis, R.E., Posada, J.A., Redrow, J.B., Celik, I.B., Chen, B.T., Beezhold, D.H., 2010. Clin. Infect. Dis. 50 (5), 693–698.
Liu, C., Yang, Y., Gao, Y., Shen, C., Ju, B., Liu, C., Tang, X., Wei, J., Ma, X., Liu, W., Xu, S., Liu, Y., Yuan, J., We, J., Liu, Z., Zhang, Z., Wang, P., Liu, L., 2020. bioRxiv.
Nassar, M.S., Bakhrebah, M.A., Meo, S.A., Alsuabeyl, M.S., Zaher, W.A., 2018. Eur. Rev. Med. Pharmacol. Sci. 22 (15), 4956–4961.
Nayak, D.P., Balogun, R.A., Yamada, H., Zhou, Z.H., Barman, S., 2009. Virus Res. 143 (2), 147–161.
Nouri, H., Zouzou, N., Moreau, E., Dascalescu, L., Zebboudj, Y., 2012. J. Electrost. 70 (1), 20–24.
Peiris, J.S.M., Guan, Y., Yuen, K.Y., 2004. Nat. Med. 10 (12), S88–S97.
Piri, A., Kim, H.R., Hwang, J., 2020. J. Hazard Mater. 384, 121477.
Santarpia, J.L., Rivera, D.N., Herrera, V., Morwitzer, M.J., Creager, H., Santarpia, G.W., Crown, K.K., Brett-Major, D., Schnaubelt, E., Broadhurst, M.J., Lwaler, J.V., Reid, S. P., Lowe, J.J., 2020. MedRxIV.
Thermo scientific. http://www.thermo.com.cn/Resources/200802/productPDF_29656.pdf (Accessed Sep. 12 2020).
van Baalen, C.A., Jeeninga, R.E., Penders, G.H., van Gent, B., van Beek, R., Koopmans, M. P., Rimmelzwaan, G.F., 2017. Vaccine 35 (1), 46–52.
Wubulihairen, M., Lu, X., Lee, P.K., Ning, Z., 2015. Atmos. Pollut. Res. 6 (4), 556–561.
Yang, W., Elankumaran, S., Marr, L.C., 2011. J. R. Soc. Interface 8 (61), 1176–1184.
Zhu, N., Zhang, D., Wang, W., Li, X., Yang, B., Song, J., Zhao, X., Huang, B., Shi, W., Lu, R., Niu, P., Zhan, F., Ma, X., Wang, D., Xu, W., Wu, G., Gao, G.F., Phil, D., Tan, W., 2020. N. Engl. J. Med. 382, 727–733.